JOURNAL OF CATALYSIS 157, 271–282 (1995)

Influence of the Acid–Base Character of Supported Vanadium Catalysts on Their Catalytic Properties for the Oxidative Dehydrogenation of *n*-Butane

T. Blasco,* J. M. López Nieto,*,[1] A. Dejoz,† and M. I. Vázquez†

*Instituto de Tecnología Química, UPV-CSIC, Avenida de los Naranjos s/n, 46022-Valencia, Spain; and †Departamento de Ingeniería Química, Universidad de Valencia, Dr. Moliner 50, 46100-Burjasot, Spain

Received August 17, 1994; revised March 21, 1995; accepted July 18, 1995

The oxidative dehydrogenation of *n*-butane on supported vanadium catalysts has been studied. Al_2O_3, sepiolite, hydrotalcite (Mg/Al atomic ratio of 3.0), and MgO were used as supports. The vanadium content of supported catalysts was varied to obtain dispersed vanadium species. The strength and number of Lewis acid sites (determined by FTIR of adsorbed pyridine) decreases in the following trend: V/Al_2O_3 > V/Sepiolite > V/hydrotalcite > V/MgO. ^{51}V NMR spectroscopy indicates that tetrahedral V^{5+}-species (with different distortion degree and/or environment) are the main vanadium species. Temperature-programmed reduction results show that the reducibility of catalysts, determined from the onset temperature of H_2-consumption, decreases in the order V/Al_2O_3 > V/MgO (first peak) > V/Sepiolite > V/MgO (second peak) ≈ V/hydrotalcite. The catalytic activity for *n*-butane oxidation follows a trend similar to that observed in TPR, concluding that the catalytic activity is related to the reducibility of surface vanadium species in the catalysts. However, the selectivity to dehydrogenated products, as well as the distribution of C_4-olefins, can be tentatively related to the acid–base character of catalysts. Thus, the selectivities to 1-butene and butadiene decrease in the order V/MgO > V/Hydrotalcite > V/Sepiolite > V/Al_2O_3, while the selectivities to 2-butene and carbon oxides present the opposite trend.

INTRODUCTION

Supported vanadium oxides exhibit interesting catalytic properties for oxidation reactions (1–6). Differences in their catalytic behavior are generally explained on the basis of the nature and distribution of vanadium species, which are influenced by the vanadium loading and the acid–base character of the support (1–10). On supports with an acid character, i.e., SiO_2, a low interaction between vanadium species and support exists and V_2O_5 is formed at relatively low vanadium content. However, on supports with basic character, i.e., MgO, a high interaction between vanadium species and support leads to the formation of metal vanadates.

MgO-supported vanadium catalysts have been shown to be selective for the oxidative dehydrogenation (ODH) of propane and *n*-butane (11) while a poor selectivity to olefins is obtained on both unsupported (12) and supported (SiO_2, Al_2O_3, TiO_2) (13) vanadia catalysts. However, depending on the alkane feeded, other vanadium-based catalysts, such as V/sepiolite (14), V/SiO_2 (15), V/Al_2O_3 (16–18), V/Nb_2O_5 (19), VAPO-5 (20), VMgAPO-5 (21), or V-silicalite (22) are also selective catalysts in the oxydehydrogenation reactions. In all these systems (14–16, 18–22), including V/MgO catalysts (23), isolated tetrahedral V^{5+} species have been proposed as selective sites for oxydehydrogenation of alkanes.

In this sense, V/SiO_2 (24) and V/Al_2O_3 (18, 25) catalysts with low vanadium loading show a low selectivity for the oxidative dehydrogenation of *n*-butane, while these catalytic systems present high selectivities to ethene during the oxidative dehydrogenation of ethane (15, 16, 18). On the other hand, a high selectivity for the ODH of propane is observed on sepiolite-supported vanadium catalysts (14), but their catalytic properties for the ODH of *n*-butane are strongly influenced by the vanadium content (26).

The aim of this paper is to study the influence of the acid–base character of the support on the selectivity for the oxidative dehydrogenation of *n*-butane on supported vanadium catalysts free of V_2O_5 crystallites. For this purpose, MgO, hydrotalcite-type Mg–Al, silicate-type magnesium (sepiolite), and Al_2O_3 have been used as supports, since according to Noller *et al.* (27) they possess different acid–base character. As the vanadium dispersion depends on the nature of the oxide support, the vanadium content in the catalysts were optimized to obtain highly dispersed vanadium species. It will be shown that, although in all the catalysts studied here tetrahedral V^{5+} can be considered as the main vanadium species, the differences in their catalytic

[1] To whom correspondence should be addressed.

0021-9517/95 $12.00

properties can be explained by the influence of the acid–base character of the supports and/or the catalysts on the selectivity to C_4-olefins.

EXPERIMENTAL

Catalyst Preparation

Commercial Al_2O_3 (Gidler T126), natural sepiolite (from Vallecas, Spain), prepared MgO, and heat-treated hydrotalcite-type Mg–Al were used as supports and referred to as AL, SEP, MG, and HTH, respectively. MgO was obtained from magnesium oxalate by calcination in air at 700°C for 3 h (23, 28). Hydrotalcite, magnesium aluminum hydroxy-carbonate, was obtained by continuous coprecipitation of aqueous solutions of magnesium nitrate and aluminum nitrate at a constant pH of 13 and at room temperature (29). The hydrotalcite was calcined in air at 450°C for 18 h (HTH).

Supported vanadium catalysts were prepared by impregnation of the support with ammonium metavanadate (V/HTH and V/MG) or vanadyl oxalate (V/SEP) aqueous solutions, according to the preparation procedure reported previously (14, 21). V/AL catalyst was prepared by impregnation of a nonporous γ-Al_2O_3 support with a vanadyl acetylacetonate/methanol solution. Then, the solid was filtered and dried at 80°C for 16 h. In all cases, the samples were calcined at 600°C for 4 h.

Catalyst Characterization

The BET surface area of the samples, S_{BET}, was obtained in an ASAP 2000 apparatus, following the BET method from N_2 adsorption isotherms at 77 K and taken at a value of 0.164 nm^2 for the cross section of N_2.

X-ray diffraction (XRD) patterns were collected in a Philips 1060 diffractometer, equipped with a graphite monochromator, operating at 40 kV and 40 mA and using nickel-filtered Cu$K\alpha$ radiation (λ = 0.1542 nm).

Solid-state ^{51}V NMR spectra were recorded at ambient temperature on a Varian VXR-400S WB spectrometer at 105.1 MHz, using a high-speed MAS Doty probe with zirconia rotors (5 mm in diameter). The spectra were recorded with pulses of 1 μs corresponding to a flip angle of $\pi/13$, in order to avoid signal distortions of the I = $\frac{7}{2}$ nuclei. The use of Bloch decays against spin echos is the preferred method here to avoid the complication arising from varying degrees of excitation selectivity that became important with the use of longer pulse lengths needed for spin echoes. To obtain the MAS–NMR spectra, samples were spun at 7 kHz. The ^{51}V chemical shifts are referred against liquid $VOCl_3$, using a 0.16 *M* $NaVO_3$ aqueous solution, whose chemical shift is −574.3 ppm, as a secondary reference. This same solution was used to calibrate the radiofrequency power.

Infrared spectra of adsorbed pyridine were obtained in a Nicolet 710 FTIR spectrophotometer. Wafers of 10 mg cm^{-2} were mounted in a Pyrex vacuum cell fitted with CaF_2 windows. The samples were degassed at 400°C for 2 h and then cooled at room temperature (RT) to obtain the original IR spectra. Then, pyridine was admitted at room temperature and degassed for 1 h to remove the physisorbed fraction, and the spectra were taken at room temperature. Finally, pyridine was desorbed at temperatures of 150 and 250°C.

Temperature-programmed reduction (TPR) results were obtained in a Micromeritics apparatus. Samples of 10 mg were first treated in argon at room temperature for 1 h. The samples were subsequently contacted with an H_2/Ar mixture (H_2/Ar molar ratio of 0.15 and a total flow of 50 ml min^{-1}) and heated, at a rate of 10°C min^{-1}, to a final temperature of 1000°C.

Catalytic Test

The catalytic experiments were carried out in a fixed-bed, continuous stainless-steel tubular reactor (i.d. 20 mm, length 400 mm), working at atmospheric pressure. The reactor was equipped with a coaxial thermocouple for catalytic bed temperature profiling.

Catalyst samples (0.3–0.5 mm particle size) were introduced in the reactor and diluted with 8 g of silicon carbide (0.5–0.75 mm particle size) to keep a constant volume in the catalyst bed. The flow rate of the reactants was varied (100–600 cm^3 min^{-1}) to achieve different contact times (W/F = 2–40 g_{cat} h $mol_{C_4}^{-1}$), and different *n*-butane conversion levels. The feed consisted of a mixture of *n*-butane, oxygen, and helium with a constant molar ratio of 5:20:75. Experiments were carried out at 500, 525, and 550°C.

Reactants and reaction products were analyzed by on-line gas chromatography, using a Hewlett–Packard apparatus equipped with two columns in parallel: (i) 23% SP-1700 Chromosorb PAW (30 × $\frac{1}{8}$ in.) to separate hydrocarbons and CO_2 and (ii) Carbosieve-S_O (8 × $\frac{1}{8}$ in.) to separate O_2 and CO.

Blank runs showed that under the experimental conditions used in this work the homogeneous reaction could be neglected.

RESULTS

Catalyst Characterization

The surface area and chemical composition of the oxide supports and catalysts are shown in Table 1. XRD patterns of V/AL and V/SEP samples are similar to those of the corresponding support. XRD of the V/MG sample (Fig. 1a) is attributed to MgO, while from IR and Raman spectroscopies (23) the presence of a poor crystalline $Mg_3V_2O_8$ phase has also been proposed. In the case of the V/HTH

TABLE 1

Characteristics of Supports and Supported Vanadium Catalysts

Sample	S_{BET} ($m^2\ g^{-1}$)	V_2O_5 (wt%)	Atomic ratio (%)[c] V	Mg	Al	Si
MgO	140	0	—	100	—	—
V/MG	108	20.0	10.0	90.0	—	—
HTH[a]	196	0	—	73.0	27.0	—
V/HTH	166	27.0	8.5	67.0	24.5	—
Sepiolite[b]	139	0	—	38.3	1.1	60.6
V/SEP	82.4	6.7	4.1	36.8	1.0	58.1
Al_2O_3	188	0	—	—	100	—
V/AL	160	7.0	4.4	—	95.6	—

[a] Heat-treated hydrotalcite type.
[b] Natural Sepiolite. Chemical composition as in Ref. (12).
[c] Chemical analysis of the elements was done by atomic absorption spectrometry.

sample (Fig. 1b), a diffuse diffraction pattern of MgO is observed. This spectrum is similar to pure hydrotalcite calcined at 600°C (29), and it corresponds to the thermal decomposition of hydrotalcite.

a. ^{51}V NMR Spectroscopy. Previous ^{51}V NMR studies

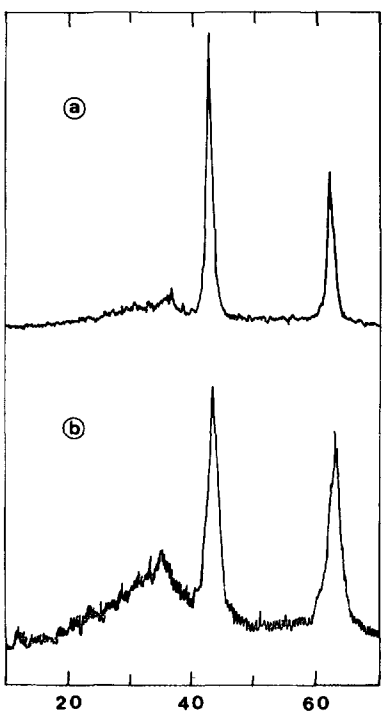

FIG. 1. XRD patterns of V/MG (a) and V/HTH (b) catalysts.

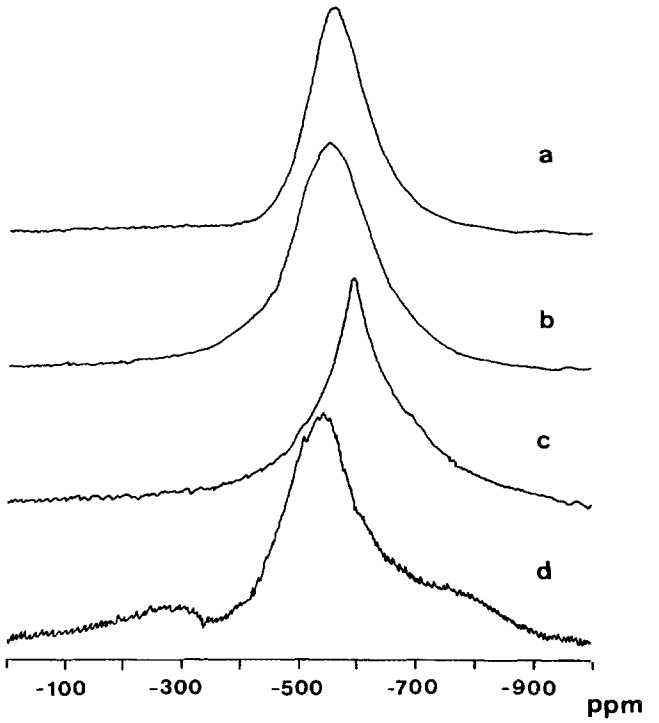

FIG. 2. ^{51}V wideline NMR spectra of V/MG (a), V/HTH (b), V/SEP (c), and V/AL (d) catalysts.

(30–34) have shown that the line shape of the $(+\frac{1}{2} \rightarrow -\frac{1}{2})$ central transition in the static spectra are dominated by chemical shift anisotropy. Thus, the combination of wideline and MAS experiments allows us to obtain reliable information on the symmetry environment of V atoms. Figures 2 and 3 show the wideline and MAS ^{51}V NMR spectra, respectively.

Figure 2a shows the ^{51}V wideline spectrum of the V/MG catalyst. The spectrum is constituted by a main line at around −555 ppm slightly asymmetric. The absence of a component in the region between −300 and −450 ppm indicates that distorted octahedral species like in MgV_2O_6 or square pyramidal like in V_2O_5 are not formed (30–32). Apart from this, no further details can be extracted from the static spectrum. The MAS–NMR spectrum, shown in Fig. 3a, can be interpreted, on the basis of previous works (32, 33), as due to the superimposition of two signals at −554 ppm (signal A) and at −570 ppm (signal B). A spectrum similar to that shown in Fig. 3a has been reported by Lapina *et al.* (32), who attributed the peak at −554 ppm to be magnesium orthovanadate, $Mg_3V_2O_8$, phase, and the shoulder at −580 ppm to associated V^{5+} octahedra or associated V^{5+} tetrahedra (δ_1 = −440 ppm, δ_2 = −570 ppm and δ_3 = −700 ppm with δ_{iso} = −570 ppm). However, since the lineshape and -width of the wideline spectrum shown in Fig. 2a strongly suggest the absence of major amounts of octahedral vanadium and the relative intensity

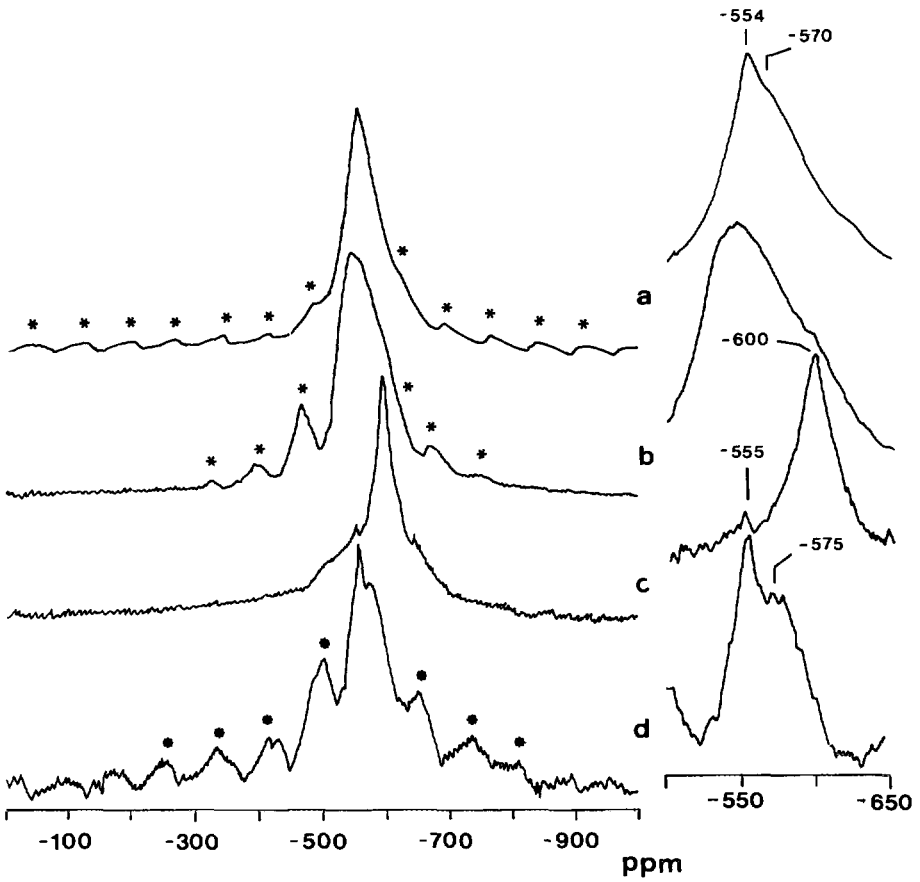

FIG. 3. ^{51}V MAS-NMR spectra of V/MG (a), V/HTH (b), V/SEP (c), and V/AL (d) catalysts. Right: corresponding enlarged spectra.

of signal B ($\delta \sim -570$ ppm) decreases with the vanadium coverage, we think that this signal must correspond to distorted VO_4 units highly dispersed on the MgO surface.

Both static (Fig. 2b) and MAS (Fig. 3b) spectra for the V/HTH sample resemble that of the V/MG sample although with a broader linewidth, indicating that V^{5+}-species must be in a tetrahedral environment. The lineshape suggests the presence of a broad range of V-environments, possibly with a different number of nonbridging oxygen atoms. This heterogeneity of V-sites distribution with different chemical shift anisotropy is also supported by the fact that the separation between the side bands maxima are not exactly the same (34) (see Fig. 3b).

The ^{51}V-wideline and MAS-NMR spectra of the V-SEP catalyst are shown in Figs. 2c and 3c, respectively. ^{51}V-wideline gives an unstructured line with little resemblance to the spectra obtained for bulk binary magnesium vanadates (30–32). The spinning spectrum is formed by the superimposition of a very broad band (signal C) and a sharper one centered at around -600 ppm (signal D). Both the spectroscopic parameters and the notation behavior of this band C led to Occelli *et al.* (31) to attribute it to a dimeric $V_2O_7^{4-}$-group in the form of a disordered surface phase. The characteristics of line D under static and spinning conditions indicate that it must be due to some type of tetrahedral V^{5+}-species. Although its chemical shift value is quite close to site 1 in α-$Mg_2V_2O_7$ (31), it is not clear if it corresponds to monomeric or dimeric species. The relatively broad lineshape of this peak must be related to the presence of a variety of chemical shifts, i.e., tetrahedral V^{5+}-sites with somewhat different symmetry.

The wideline spectrum of the V/AL catalyst is constituted by three main components at around -300 ppm, -540 ppm, and -800 ppm (Fig. 2d). Similar spectra are observed by other authors (17, 30, 34). Under spinning conditions, two lines are observed at -555 ppm and -575 ppm (Fig. 3d).

The peak at around -300 ppm (signal E) in the static spectrum (Fig. 2d) clearly indicates the presence of octahedral V^{5+}-species (30, 34). However, the low intensity of the octahedral species in the V/AL sample studied here makes it difficult to establish further details on the vanadium coordination geometry.

The spectral parameters of a signal centered at -540

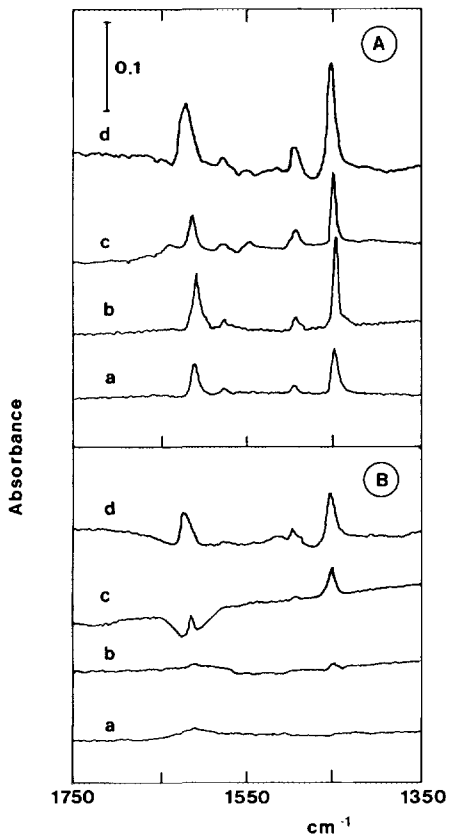

FIG. 4. FTIR spectra of pyridine adsorbed on V/MG (a), V/HTH (b), V/SEP (c), and V/AL (d) samples obtained at evacuation temperatures of 150°C (A) and 250°C (B).

ppm in the wideline spectrum of V/Al_2O_3 has been attributed to VO_4 tetrahedron bonded to two other V-atoms via oxygen atoms forming chains (30). Following the $Q^{(n)}$ notation, where n is the number of bridging oxygen atoms connecting two V-polyhedra, these VO_4-tetrahedra would be of $Q^{(2)}$ type. Lapina *et al.* (33) attributed the lines in the chemical shift range between −520 ppm and −590 ppm to VO_4-species bound to the alumina surface via one or two oxygen atoms and with H_2O molecules in their second coordination sphere, in a very regular tetrahedral environment. The MAS–NMR spectrum of our V/AL catalyst shown in Fig. 3d presents two sharp peaks at −555 (signal F) and −575 (signal G) ppm, which must correspond to V^{5+}-tetrahedra with a different geometry. Comparison with model compounds suggests that the resonance at −555 ppm must be due to isolated V^{5+} in a very regular tetrahedral symmetry, in agreement with the assignment of Lapina *et al.* (33). The chemical shift value of signal G under spinning and the static spectrum (with two components probably corresponding to δ_2 and δ_3 at −540 ppm and −800 ppm, respectively) suggest its attribution to the formation of VO_4-chains ($Q^{(2)}$-type species) like in metavanadates NH_4VO_3 or $NaVO_3$ (30).

b. Catalyst acidity. Figure 4 illustrates the infrared spectra of pyridine adsorbed on the supported vanadium catalysts after evacuation at temperatures of 150°C (Fig. 4A) and 250°C (Fig. 4B). Bands at 1450, 1493, and 1609 cm^{-1} (1620 cm^{-1} for the V/AL sample), characteristics of pyridine retained on Lewis acid sites, are observed at an evacuation temperature of 150°C. However, after evacuation at 250°C these bands are only present, with a low intensity, in the spectra of the V/AL and V/SEP samples. Furthermore, the band at 1545 cm^{-1} associated to pyridine adsorbed on Brønsted acid sites, is only observed in the spectra of V/AL and V/SEP samples at an evacuation temperature of 150°C.

As the intensity of the band at 1450 cm^{-1} is related to the number of Lewis acid sites, it can be concluded that:

(i) The number of Lewis acid sites decreases according the following trend: V/AL > V/SEP > V/HTH > V/MG.

(ii) The strenghth of Lewis acid sites on V/AL or V/SEP is higher than on V/HTH or V/MG catalysts.

(iii) Brønsted acid sites are only observed on V/SEP and V/AL catalysts.

c. Temperature-programmed reduction. The temperature-programmed reduction profiles of supported vanadium catalysts are shown in Fig. 5. Except in the case of the V/MG sample, in which two peaks are observed, the TPR profiles of the catalysts exhibit only one prominent maximum. The onset temperature, T_{onset}, and the temperature of the maximum hydrogen consumption, T_M, are listed in Table 2. In all cases the amount of hydrogen consumed during the TPR experiment was approximately 1.0 mol-H_2 mol^{-1} of vanadium.

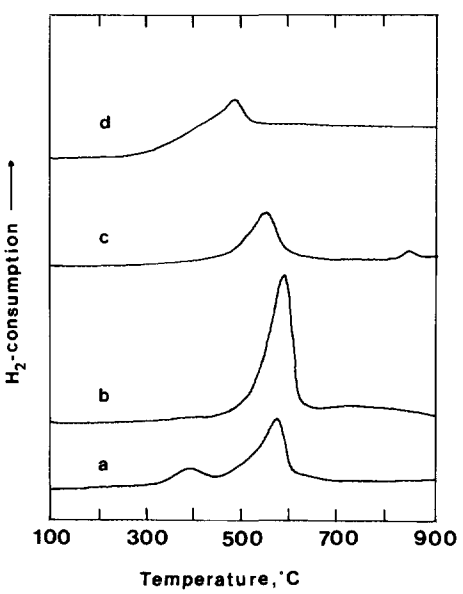

FIG. 5. TPR profiles of supported vanadium catalysts: V/MG (a), V/HTH (b), V/SEP (c), and V/AL (d).

TABLE 2

TPR Results of Supported Vanadium Catalysts

Sample	T_{onset} (°C)	T_M (°C)
V/AL	300	465
V/SEP	410	535
V/HTH	421	585
V/MG	310	373
	450	568

TPR results of monolayer and double-layer supported vanadium catalysts indicate (35) that the reducibility decreases in the sequence $V/TiO_2 > V/Al_2O_3 > V/SiO_2 > V/MgO$. In addition, it was observed that the T_M, i.e., the temperature of the maximum, increases with the vanadium loading for V/MgO catalysts. However, Iwamoto *et al.* (36) observed four peaks in the TPR profile of a MgO-supported vanadium sample, which were attributed to two types of vanadium species reduced in two step, i.e., $V_2O_5 \rightarrow V_2O_4$ and $V_2O_4 \rightarrow V_2O_3$. Two different vanadium species have also been proposed in MgO-supported vanadium catalysts prepared by impregnation of magnesium oxalate with an aqueous vanadyl oxalate solution (26). These V–Mg–O catalysts present TPR patterns similar to that shown in Fig. 5a and they are associated to (26): (i) isolated V^{5+}-species in a distorted VO_4 tetrahedral environment on the catalyst surface and (ii) isolated V^{5+}-species in a $Mg_3V_2O_8$-structure in the bulk of the catalyst. We must note that the presence of two different vanadium species is only observed on catalysts with vanadium contents lower than 30 wt%, while the number of isolated V^{5+}-species in a crystalline $Mg_3V_2O_8$-phase increases with the vanadium content. In addition, from the comparison between catalyst characterization and catalytic properties, it has been proposed that the catalytic activity of the V/MG sample is mainly related to isolated V^{5+}-species with high reducibility (26).

According to the results shown in Table 2 it can be concluded that the T_{onset} increases in the order V/AL ≤ V/MG (first peak) < V/SEP ≤ V/HTH < V/MG (second peak), while the T_M increases in the order V/MG (first peak) < V/AL < V/SEP < V/MG (second peak) < V/HTH. Since the temperature at which the maximum hydrogen consumption is observed depends on the V-content and probably on the dispersion, the reducibility of the catalysts can be better reflected by the onset temperature.

d. Catalytic Study. The catalytic results obtained during the oxidative dehydrogenation of *n*-butane on supported vanadium catalysts are shown in Table 3. C_4-Olefins (including 1-butene, *cis*-2-butene, *trans*-2-butene, and butadiene), CO, and CO_2 are the main reaction products, while C_2- or C_3-hydrocarbons are obtained as minority ones. Oxygen-containing products other than carbon oxides were not observed.

Figure 6 shows the variation of the conversion of *n*-butane with the contact time (*W/F*). From these results it can be concluded that the catalytic activity per gram of catalyst decreases in the order: V/AL > V/Mg > V/HTH > V/SEP. A similar trend is obtained when specific activities (calculated per square meter of surface) are considered.

However, because the catalysts have a different vanadium content, their catalytic activity per mole of vanadium were calculated and they are shown in Table 3. It can be seen that the activity of vanadium atoms decrease in the following trend: V/AL > V/MgO ≈ V/SEP > V/HTH.

In Table 3 it can also be seen that at low reaction temperature and a conversion of *n*-butane about 10%, selectivities to C_4-olefins higher than 50% are obtained on all the catalysts. On the V/MG, V/HTH, and V/SEP catalysts it can be seen that both the conversion of *n*-butane and the selectivity to oxydehydrogenated products increases when increasing the reaction temperature, while for the V/AL sample the higher the reaction temperature the higher the *n*-butane conversion and the lower the selectivity to dehydrogenated products.

Figures 7 and 8 show the variation of the selectivities to C_4-olefins with the conversion level of *n*-butane obtained at 500 and 550°C, respectively. Some of these results are also summarized in Table 4, in which the selectivities to each of the reaction products have been

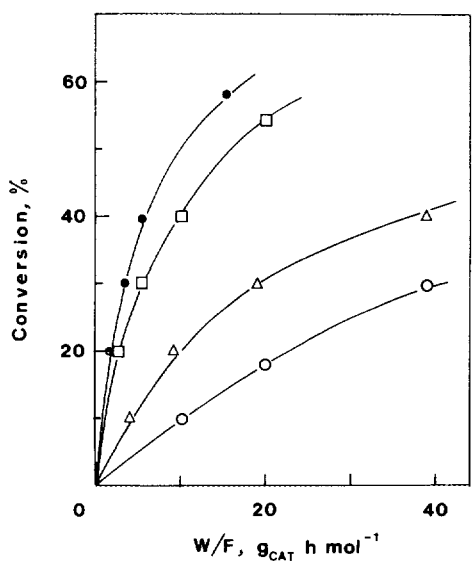

FIG. 6. Variation of the conversion of *n*-butane with the contact time, W/F, obtained at a reaction temperature of 550°C. (□) V/MG; (○) V/HTH; (△) V/SEP; (●) V/AL.

TABLE 3
Oxidative Dehydrogenation of *n*-Butane on Supported Vanadium Catalysts

Sample	W/F[a]	*T* (°C)	Conversion (%)	Catalytic activity (mol C_4 h^{-1} g_{cat}^{-1})	TOF (mol C_4 h^{-1} mol-V^{-1})	Selectivity (%) ODH[b]	CO	CO_2	Others[c]
V/MG	4.1	500	11.2	2.73	12.4	58.6	9.7	29.4	2.3
		525	17.6	4.29	19.5	62.0	9.9	26.1	2.0
		550	25.7	6.27	28.5	61.2	10.7	26.2	1.9
V/HTH	10	500	10.9	1.09	3.63	50.4	12.8	33.2	3.6
		525	16.6	1.66	5.53	53.5	13.0	29.8	3.7
		550	22.7	2.27	7.57	54.9	12.7	29.1	3.3
V/SEP	20	500	10.6	0.53	14.3	49.1	22.1	26.0	2.9
		525	14.0	0.70	18.9	52.3	20.9	24.1	2.7
		550	19.0	0.95	25.7	48.5	23.9	24.6	2.9
V/AL	2.3	500	9.9	4.30	113	53.7	21.8	21.8	2.7
		525	16.1	7.00	184	45.2	28.6	24.0	2.2
		550	26.0	11.3	297	34.9	36.4	26.6	2.1

[a] Contact time, W/F in g_{cat} h (mol C_4)$^{-1}$.
[b] Selectivity to C_4-olefins (1-butene, 2-butenes, and butadiene).
[c] C_2- and C_3-hydrocarbons.

included. It can be seen that, independently of the reaction temperature, the selectivities to 1-butene on V/MG and V/HTH catalysts are higher than on V/SEP and V/AL catalysts. In all the cases, 1-butene can be considered as a primary and unstable product (Figs. 7 and 8).

The selectivity to 2-butenes (*cis*- and *trans*-2 butene) decreases with the *n*-butane conversion. For this reason, 2-butenes can be considered as primary (unstable) products (Figs. 7 and 8). At low reaction temperature, i.e., 500°C, the selectivity to 2-butene on V/SEP and V/AL is higher than that on V/MG and V/HTH catalysts. However, at higher reaction temperatures, similar selectivities are obtained on any catalysts. It is noted that

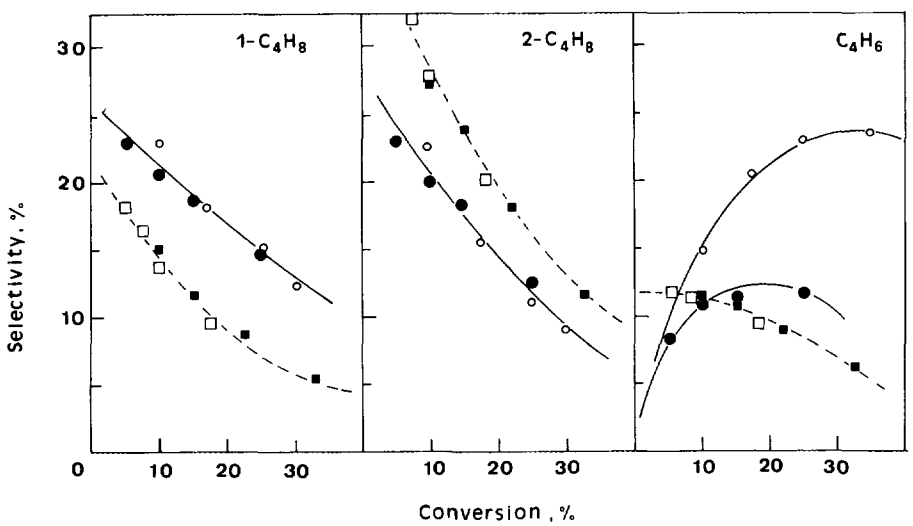

FIG. 7. Variation of the selectivities to 1-butene, 2-butenes, and butadiene with the conversion of *n*-butane obtained at a reaction temperature of 500°C. (○) V/MG; (●) V/HTH; (□) V/SEP; (■) V/AL.

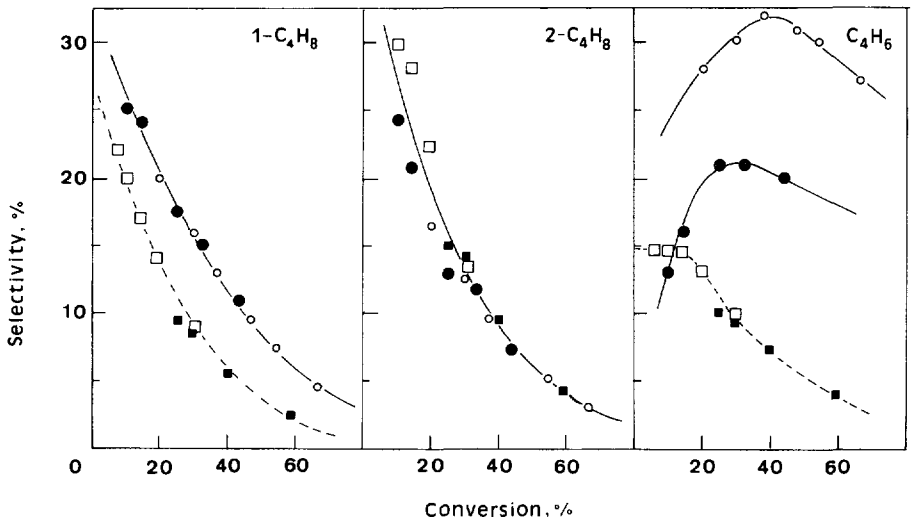

FIG. 8. Variation of the selectivities to 1-butene, 2-butenes, and butadiene with the conversion of *n*-butane obtained at a reaction temperature of 550°C. Symbols as in Fig. 7.

trans-2-butene/*cis*-2-butene molar ratios higher (V/AL and V/SEP) or lower (V/MG and V/HTH) than 1 were obtained (Table 4).

The variation of the selectivity to butadiene with the *n*-butane conversion on supported vanadium catalysts can be seen in Figs. 7 and 8. For V/MG and V/HTH catalysts, the selectivity to butadiene increases when increasing the *n*-butane conversion, reaching a maximum for a value of 40%. However, for V/SEP and V/AL catalysts the selectivity to butadiene decreases when

TABLE 4

Variation of Selectivity to C_4-Olefin with the Reaction Temperature and Conversion of *n*-Butane

Sample	W/F[a]	Temperature (°C)	Conversion (%)	Selectivity						
				1-C_4H_8	*t*-2-C_2H_8	*c*-2-C_4H_8	C_4H_6	CO	CO_2	Others[b]
V/MG	4.1	500	11	21.6	9.2	11.2	16.6	9.7	29.4	2.3
	10	500	22	18.4	7.2	8.8	20.3	10.5	33.0	1.8
	2.7	550	21	20.1	7.5	9.3	28.0	9.6	23.3	2.2
	10	550	43	10.9	3.3	4.0	31.8	13.7	34.9	1.4
V/HTH	10.0	500	11	20.6	9.3	10.6	9.9	12.8	33.2	3.6
	22.0	500	17	17.9	7.6	8.7	11.8	14.1	37.0	2.9
	10.0	550	23	19.2	7.9	8.9	19.9	12.7	29.1	3.3
	39	550	43	11.0	3.7	4.4	20.3	16.4	41.6	2.6
V/SEP	20	500	11	13.6	14.1	11.0	10.3	22.1	26.0	2.9
	40	500	18	9.4	10.6	8.2	8.8	28.3	32.5	2.2
	20	550	19	13.7	12.1	9.9	12.9	23.9	24.6	2.9
	39	550	31	8.4	7.8	6.3	10.0	31.5	33.5	2.5
V/AL	2.3	500	10	15.0	14.6	12.5	11.6	21.8	21.8	2.7
	5.4	500	18	8.7	9.1	7.5	8.5	32.1	32.1	2.0
	1.8	550	20	9.5	8.2	6.9	10.2	36.9	26.6	1.7
	5.4	550	39	5.6	5.3	4.4	7.2	44.3	31.1	2.1

[a] Contact time, W/F in g_{cat} h $(mol_{C4})^{-1}$.
[b] C_2- and C_3-hydrocarbons.

increasing the conversion of *n*-butane. Thus, on V/SEP and V/AL catalysts butadiene can be considered a primary and unstable product, while on V/MG and V/HTH catalysts butadiene can mainly be considered a secondary and unstable product.

In general, the selectivities to CO and CO_2 decrease when increasing the reaction temperature, except for the V/AL catalysts in which the selectivity to CO increases with the reaction temperature (Table 4). In addition, it can also be observed that the CO/CO_2 ratio increases in the following trend: V/MG < V/HTH < V/Sep < V/Al.

DISCUSSION

Nature of Vanadium Species

The final surface vanadium concentration on supported vanadium catalysts depends on the vanadium content but also on possible modifications of the support during the impregnation and/or calcination steps. In this way, MgO is transformed into $Mg(OH)_2$ when the impregnation is carried out in the presence of water (23, 28). As a consequence, vanadium is partially occluded in the bulk of the catalyst after calcination, resulting in a lower surface vanadium concentration, as concluded from the differences between surface and bulk V/Mg atomic ratios (23). In the sepiolite-supported vanadium catalyst, the initial $Mg_8Si_{12}O_3$ $(OH)_4$ crystalline phase is transformed into $MgSiO_3$ to a degree that depends on the vanadium content and calcination temperature (14, 26). This process is accompanied by a decrease on the surface area (Table 1). For the hydrotalcite-supported catalyst the formation of a low-crystalline MgO after calcination can be proposed.

The vanadium dispersion and the formation of V_2O_5 and/or metal vanadates on supported vanadium catalysts depend on the chemical properties of the metal oxide used as support. In general, it has been observed (7–10) that the degree of interaction between the vanadium atoms and the support, as well as the vanadium content required to form crystalline V_2O_5, increase when decreasing the acid character of the support. The four supports used in the present publication possess different acidic properties. Calcined hydrotalcite has been reported (39) to be less basic than MgO, while their acid sites, attributed to Al^{3+} located in a MgO lattice, are weaker than in alumina. These results are in good agreement with those reported by Noller *et al.* (27), who found that the acidity of pure and mixed metal oxides increases in the order MgO < hydrotalcite-type Mg–Al < Mg silicate (as Sepiolite) < Al_2O_3. Taking into account these considerations and in order to obtain high vanadium dispersion, lower amounts of vanadium were supported on SEP and AL than on MG and HTH supports.

The ^{51}V NMR results indicate that the vanadium coordination is predominantely tetrahedral (four coordinated) in all the catalysts, although the type of V^{5+}-species formed depends on the characteristics of the support. On the most basic catalysts studied here, i.e., V/MG, two types of V^{5+}-species without bridging V–O–V oxide ions ($Q^{(0)}$ type) are observed: well-dispersed VO_4-tetrahedron and $Mg_3V_2O_8$ like (26). The V^{5+}-species formed on MgO can be understood on the basis of the strong interaction between the V-atoms and the support leading to highly dispersed vanadium species at low converages and to the formation of crystalline V–Mg vanadates when the vanadium content increases.

On the most acid catalyst in the present work, i.e., V/AL catalyst, we observe the presence of isolated V^{5+}-tetrahedra, chains of V^{5+}-tetrahedra ($Q^{(2)}$-type species), and small amounts of octahedral V^{5+}-species. These results are in agreement with those previously reported for V/Al_2O_3 catalysts with vanadium loading under the monolayer (30, 34). In fact, it has been observed that for V/Al_2O_3 catalysts, the V-environment goes from tetrahedral at low coverages to octahedral at high coverages (30) and finally to the formation of crystalline V_2O_5 above 60% of the theoretical monolayer (10). This suggests a much weaker interaction between the vanadium atoms and the oxide support than on V/MgO catalysts, due to the higher acidity of the Al_2O_3, which favors the association of the vanadium atoms.

An intermediate degree of vanadium aggregation can be expected in V/HTH and V/SEP with intermediate acid character. Although the characteristics of the V/HTH catalyst resemble that of V/MG catalyst, the ^{51}V NMR spectra of the former suggest a higher heterogeneity of vanadium sites. In fact, tetrahedral V^{5+}-species with different number of bridging oxygen seem to be present in the V/HTH sample. On the other hand, dimeric V^{5+}-species are detected mainly on the V/SEP catalyst, in agreement with previous studies (31).

To summarize, in accordance with previous works (14, 26) it can be concluded that the degree of association of vanadium species on V/SEP or V/HTH is higher than that on V/MG and lower than that on V/AL, in agreement with the acid character of the oxide support. The presence of Mg–O–Al and Mg–O–Si pairs, in addition to Mg–O–Mg pairs, in calcined hydrotalcite (37) and sepiolite (14), respectively, modifies the interaction of the Mg sites with the vanadium atoms leading to V^{5+}-species different than those observed on MgO. Since the Mg/Si atomic ratio in sepiolite is lower than the Mg/Al atomic ratio in hydrotalcite, the number of Mg–O–Mg sites must be higher in the latter. According to this, the higher concentration of heterogeneous (Mg–O–Si) pairs in V/SEP favor the formation of V–O–V dimers that are not the majority in V/HTH.

Catalytic Activity

It is known that a correlation between catalytic activity in oxidation reactions and reducibility of catalysts exist (5, 10, 38–40). However, the factors determining the reducibility of vanadium species are still unclear. Haber *et al.* (39)

concluded that the structure of the vanadium–oxygen species determines the number of removable oxygen for each vanadium atom. More recently, Deo and Wachs (40) have proposed that the strength of the bridging V–O–support bond controls the reducibility and reactivity of the supported vanadium catalysts.

Since the ODH reaction must involve redox sites, the catalytic activity must be related with the reducibility of the V^{5+}-species. When the onset temperature of the TPR patterns are considered, the catalysts' reducibility decrease in the order V/AL > V/MG (first peak) > V/SEP > V/HTH ≈ V/MG (second peak) (Table 2). On the other hand, when the vanadium loading is considered, the catalytic activity (mol C_4/mol V) of catalysts decreases in the order: V/AL > V/MG ≈ V/SEP > V/HTH. Thus, a parallelism between reducibility and the catalytic activity can be proposed.

The study of V_2O_5/MgO catalysts with different V-contents (26) has shown a correlation between the area of the low-temperature peak in the TPR patterns and the catalytic activity for the ODH of propane and *n*-butane. Furthermore, it has been observed that on V–Mg–O catalysts the high catalytic activity for the ODH reactions is associated to the presence of the NMR peak at −570 ppm, signal B (41). These results suggest that the higher catalytic activity of V/MgO catalyst with respect to the V/HTH sample must be due to the presence of highly dispersed tetrahedral V^{5+}-species (signal B) easily reducible, since these species are less abundant, if present, on V/HTH. On the other hand, the catalyst reducibility can also depend on the nature of the support. In this way, the presence of Mg–O–Me sites (in which Me can be Mg but also Al in hydrotalcite or Si in sepiolite) modifies the acid–base character of the support and the possible V–O–support interaction.

In the case of V/AL, different vanadium species, with high reducibility, are observed. A weaker interaction between the V-atoms and the support than in V/MG, and then a much weaker V–O–support bond could favor the reducibility of the vanadium surface species, in agreement with previously reported data for selective oxidation reactions (40).

Taking into account all these considerations, it can be proposed that the catalytic performance of the supported-vanadium catalysts in the ODH of *n*-butane is determined by a variety of factors, for example, the structure of vanadium species or the V–O–support interaction, which are mainly dependent on the nature of the support. To clearly establish the nature of active sites and all the effects controlling the catalyst activity, a more detailed study with different degrees of coverages for different supports is required.

Influence of the Acid–Base Character of the Catalysts on the Selectivity to Oxydehydrogenated Products

The overall selectivity to dehydrogenated products at low and high *n*-butane conversion (Fig. 9) follows the same trend as the selectivities to 1-butene and butadiene, i.e.,

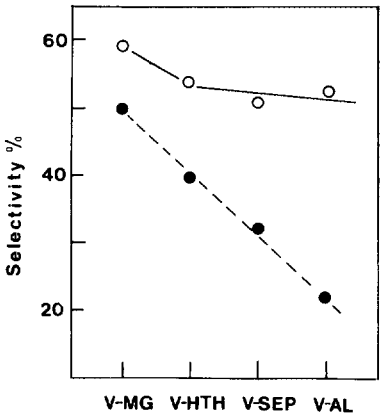

FIG. 9. Selectivity to C_4-olefins for the ODH of *n*-butane on supported vanadium catalysts obtained at 500°C and an *n*-butane conversion of 10% (○), and 550°C and an *n*-butane conversion of 30% (●).

V/MG > V/HTH > V/SEP > V/AL, while the opposite is observed for the selectivities to 2-butenes and carbon oxides. Since the number and strength of acid sites increase in the sequence V/MG < V/HTH < V/SEP < V/AL, it seems reasonable to think that the distribution of C_4-olefins, as well as the influence of the reaction parameters (such as temperature and conversion of *n*-butane) on the selectivity to dehydrogenated products depend on the acid character of the catalysts.

From the variation of the selectivities to C_4-olefins with the *n*-butane conversion (Figs. 7 and 8) two different networks for the oxidative dehydrogenation of *n*-butane can be proposed depending on the acid character of the catalysts (Scheme 1). On V/MG and V/HTH catalysts (Scheme 1a) mono-olefins are directly formed from *n*-butane, while butadiene is mainly formed by consecutive reactions. However, on V/SEP and V/AL catalysts mono- and di-olefins are directly formed, and their consecutive reactions pro-

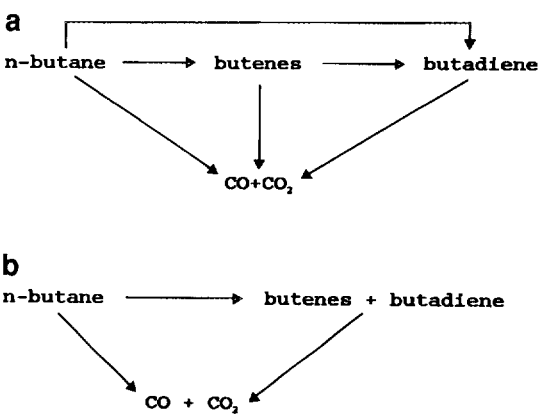

SCHEME 1. Possible reaction networks of the oxidative dehydrogenation of *n*-butane.

duce carbon oxides (Scheme 1b). Therefore, the selectivity to dehydrogenated products will be determined by the rate of parallel and consecutive reactions.

According to the proposed mechanism (12, 42), *n*-butane first reacts by dissociation of a methylene C–H bond to form a secondary butyl radical. This step is generally accepted to be the rate-determining step. After a second H-abstraction, olefinic intermediates are formed and subsequently desorbed as olefins:

$$n\text{-butane} \xrightarrow{1} [\text{butyl species}] \xrightarrow{2} [\text{butene intermediate}] \xrightarrow{3} \text{butenes}$$

In this way, it is obvious that if steps 2 and 3 are rapid, the selectivity to olefins must be high. However, slow rates for these steps can favor a deeper oxidation.

It has been previously proposed (12) that the high selectivity to 1-butene on the oxidative dehydrogenation of *n*-butane on V/MgO catalysts is related to the high rate of the second hydrogen abstraction, producing a 1-butene/*cis*-2-butene/*trans*-2-butene molar ratio closer to a statistical distribution (3/1/1) than an equilibrium ratio (1/1/1.1).

In the present work, a C_4-olefin distribution similar to the statistical ratio is observed on V/MG or V/HTH catalysts while on V/SEP or V/AL catalysts the C_4-olefins distribution is similar to the equilibrium ratio. Assuming that the rate of the second H-abstraction (step 2) is the selectivity-determining step (43), the results obtained here suggest that this is slower for acid catalysts, allowing the product distribution to attain the equilibrium.

Another possible selectivity-determining step to be considered is the desorption of the olefinic intermediates (step 3), which will be mostly determined by the interaction of the olefins with the catalyst surface. As previously proposed in partial oxidation reactions (3), this interaction will depend on the acid–base character of both the products and the catalyst. According to Dadyburjor *et al.* (3), olefins (electron-donating molecules) have a higher basic character than the corresponding paraffins. Olefins will interact more strongly with acid catalysts than with basic ones. This stronger interaction will decrease the desorption rate of the adsorbed olefins (step 3) favoring, at low *n*-butane conversions, high selectivities to 2-butene and butadiene and a C_4-olefins distribution closer to equilibrium ratio, in agreement with our results (Table 4).

For this reason, steps 2 and/or 3 can be proposed as selectivity-determining steps at low conversion of *n*-butane.

At high *n*-butane conversion, consecutive reactions can also depend on the acid–base character of the catalysts. Thus, in addition to oxydehydrogenation reactions, isomerization or deep oxidation of the olefins directly formed from *n*-butane can also take place.

The results of Table 4 suggest that the most important consecutive reaction on V/SEP and V/AL catalysts is the formation of carbon oxides, while on V/MG and V/HTH catalysts the formation of butadiene by oxidative dehydrogenation of the formed olefins is favored. This is in agreement with previous results, since it has been reported that 1-butene is transformed to butadiene with high selectivity on V/MgO catalysts (44) while on V/Al_2O_3 catalysts it is oxidized to carbon oxides (on catalysts with low vanadium content) or maleic anhydride (at high vanadium content) (45).

The isomerization of 1-butene on V- (46) or Mo-based (47) catalysts increases when increasing their acid character. In this way, it has been proposed that the presence of acid sites are responsible for the isomerization (at low reaction temperature) and extensive oxidation (at high reaction temperature) of 1-butene (47). Recently, Busca *et al.* (48) have studied the interaction of saturated and unsaturated C_4-hydrocarbons on V/MgO, V/TiO_2, or V–P–O. They found that the catalytic properties of these catalysts depend on the efficiency of the different active sites. The high selectivity in oxydehydrogenation products obtained on V/MgO catalyst is explained on the basis of its low activity in the successive transformation of olefins and dienes.

From our results it can be concluded that the oxidative dehydrogenation of *n*-butane and 1-butene is favored on catalysts with a basic character. In this case, the weak hydrocarbon–catalyst interaction proposed by Busca *et al.* (48) can explain the high selectivity to olefins and dienes and the low selectivity to carbon oxides.

On the other hand, a strong hydrocarbon–catalyst interaction is expected on acid catalysts (48). If, as on V/TiO_2, V/Al_2O_3 (with high vanadium content), or V–P–O catalysts, oxygen-insertion sites, i.e., vanadyl species (V = 0 double bonds), are present, partial oxygenated products are obtained. But if, as on the catalysts studied here (V/AL or V/SEP), vanadyl species are not present, butenes are initially formed but, due to the strong hydrocarbon–catalyst interaction, they transform to carbon oxides at high butane conversions.

CONCLUSIONS

In conclusion, tetrahedral V^{5+} are the main vanadium species on all the catalysts studied here, with a dispersion degree that depends on the acid character and/or the heterogeneity of the support. The catalytic activity is related to the ease reduction of supported vanadium oxide catalysts. However, the C_4-olefins distribution and the selectivity to dehydrogenated products strongly depend on the acid–base character of the catalyst surface. Catalysts with a basic character, i.e., V/MG and V/HTH samples, favor both the initial formation of 1-butene and its further conversion to butadiene. In opposition, on catalysts with an acid charac-

ter, butenes and butadienes are initially formed (with a high content of 2-butenes), but then carbon oxides are formed mainly by consecutive reactions.

In this way, the importance of the acid–base character of the catalysts on the type of both parallel and consecutive reactions during the oxidative dehydrogenation of *n*-butane has been shown. The second H-abstraction and/or the desorption of olefinic intermediates can be considered as the selectivity-determining steps. The desorption rate of olefinic intermediates from catalysts with acid character must be lower than that from catalysts with basic character, and then, one must expect a C_4-olefin distribution near equilibrium (2-butenes/1-butene molar ratio higher than 1) on acid catalysts and high selectivity to 1-butene on catalysts with basic character. Furthermore, on catalysts with acid character, olefins are strongly adsorbed favoring its oxidation to carbon oxides which are the most important products, while on catalysts with basic character, butadiene is the main product formed from consecutive reactions.

ACKNOWLEDGMENT

Financial support from the Comisión Interministerial de Ciencia y Tecnología in Spain (MAT 607/91) is greatly appreciated.

REFERENCES

1. Wainwright, M. S., and Foster, N. R., *Catal. Rev.-Sci. Eng.* **19,** 211 (1979).
2. Bielanski, A., and Haber, J., *Catal. Rev.-Sci. Eng.* **19,** 1 (1979).
3. Dadyburjor, D. B., Jewur, S. S., and Ruckenstein, E., *Catal. Rev.-Sci. Eng.* **19,** 293 (1979).
4. Gellins, P., *in* "Catalysis" (G. C. Bond and G. Webb, Eds.), Specialist Periodical Report, Vol. 7, p. 105, Royal Chem. Soc., London, 1985.
5. Bond, G. C., and Tahir, S. F., *Appl. Catal.* **71,** 1 (1991).
6. Oyama, S. T., *Res. Chem. Intermed.* **15,** 165 (1991).
7. Miyamoto, A., and Mori, K., *in* "Proceedings, 7th International Congress on Catalysis, Tokyo, 1980" (T. Seiyama and K. Tanabe, Eds.), p. 1344. Elsevier, Amsterdam, 1981.
8. Roozeboum, F., Mitlelmeijer-Hazeleger, M. C., Moulijn, J. A., Medema, J., de Beer, V. H. J., and Gellins, P. J., *J. Phys. Chem.* **84,** 2783 (1980).
9. Deo, G., and Wachs, I. E., *J. Phys. Chem.* **95,** 5889 (1991).
10. López Nieto, J. M., Kremenic, G., and Fierro, J. L., *Appl. Catal.* **61,** 235 (1990).
11. Kung, H. H., and Chaar, M. A., U.S. Patent 4772319 (1988).
12. Chaar, M., Patel, D., Kung, M., and Kung, H. H., *J. Catal.* **105,** 483 (1987).
13. Corma, A., López Nieto, J. M., Paredes, N., Pérez, M., Shen, Y., Cao, H., and Suib, S. L., *in* "New Developments in Selective Oxidation by Heterogeneous Catalysis" (P. Ruiz and B. Delmon, Eds.), Studies in Surface Science and Catalysis, Vol. 72, p. 213. Elsevier, Amsterdam, 1992.
14. Corma, A., López Nieto, J. M., Paredes, N., and Pérez, M., *Appl. Catal. A* **97,** 159 (1993).
15. Le Bars, J., Vedrine, J. C., Auroux, A., Trautmann, S., and Baers, M., *Appl. Catal.* **88,** 179 (1992).
16. Le Bars, J., Auroux, A., Trautmann, S., and Baers, M., *in* "Proceedings, DGMK-Conference, Selective Oxidation in Petrochemistry," p. 59, Ber.-Dtsch.Wiss.Ges.Erdoel. Erdgas Kohle, Tagungsber, 1992.
17. Eon, J. G., Olier, R., and Volta, J. C., *J. Catal.* **145,** 318 (1994).
18. Concepción, P., Dejoz, A., López Nieto, J. M., and Vázquez, M. I., *in* "Proceedings, 14th Iberoamerican Symposium of Catalysis," p. 769. Chilean Chemical Society, Concepción-Chile, 1994.
19. Smits, R. H. M., Seshan, K., and Ross, J. R. H., *J. Chem. Soc., Chem. Commun.*, 558 (1991).
20. Concepción, P., López Nieto, J. M., and Pérez-Pariente, J., *Catal. Lett.* **19,** 333 (1993).
21. Concepción, P., López Nieto, J. M., and Pérez-Pariente, J., *Catal. Lett.* **28,** 9 (1994).
22. Bellussi, G., Centi, G., Perathoner, S., and Trifiró, F., *in* "Catalytic Selective Oxidation," ACS Symp. Series, Vol. 523, p. 281. Am. Chem. Soc., Washington, DC, 1993.
23. Corma, A., López Nieto, J. M., and Paredes, N., *J. Catal.* **144,** 425 (1993).
24. Owens, L., and Kung, H. H., *J. Catal.* **144,** 202 (1993).
25. Andersen, P. J., and Kung, H. H., *in* "Proceedings, 10th International Congress on Catalysis, Budapest, 1992" (L. Guczi, Ed.), p. 205. Elsevier, Amsterdam, 1993.
26. Corma, A., López Nieto, J. M., Paredes, N., Dejoz, A., and Vázquez, M. I., *in* "New Developments in Selective Oxidation II" (V. Cortés Corberán and S. Vic Bellón, Eds.), Studies in Surface Science and Catalysis, Vol. 82, p. 113. Elsevier, Amsterdam, 1994.
27. Noller, H., Lercher, J. A., and Vinex, H., *Mater. Chem. Phys.* **18,** 557 (1988).
28. Corma, A., López Nieto, J. M., and Paredes, N., *Appl. Catal. A* **104,** 161 (1993).
29. Rey, F., Fornés, V., and Rojo, J. M., *J. Chem. Soc., Faraday Trans.* **88,** 2233 (1992).
30. Eckert, H., and Wachs, I. E., *J. Phys. Chem.* **93,** 6796 (1989).
31. Occelli, M. L., Maxwell, R. S., and Eckert, H., *J. Catal.* **137,** 36 (1992).
32. Lapina, O. B., Simakov, A. V., Mastikhin, V. M., Veniaminov, S. A., and Subin, A. A., *J. Mol. Catal.* **50,** 55 (1989).
33. Lapina, O. B., Mastikhin, V. M., Simonova, L. G., and Bulgakova, Y. O., *J. Mol. Catal.* **69,** 61 (1991).
34. Das, N., Eckert, H., Hu, H., Wachs, I. E., Walzer, J. F., and Feher, F. J., *J. Phys. Chem.* **97,** 8240 (1993).
35. Kijenski, J., Baiker, A. Glinski, N., Dollenmeier, P., and Wokaun, A., *J. Catal.* **101,** 1 (1986).
36. Iwamoto, M., Takenaka, T., Matsukami, K., Hirata, J., Kayama, S., and Uzumi, J., *Appl. Catal.* **16,** 153 (1985).
37. Mckenzie, A. L., Fishel, C. T., and Davis, R. J., *J. Catal.* **138,** 547 (1992).
38. Fierro, J. L. G., Arrua, L. A., López Nieto, J. M., and Kremenic, G., *Appl. Catal.* **37,** 323 (1988).
39. Haber, J. Kozlowska, A., and Kozlowski, R., *J. Catal.* **102,** 52 (1986).
40. Deo, G., and Wachs, J. E., *J. Catal.* **129,** 307 (1991).
41. Blasco, T., Dejoz, A., López Nieto, J. M., and Vázquez, M. I., to appear.
42. Kung, H. H., *Ind. Eng. Chem. Prod. Res. Dev.* **25,** 171 (1986).
43. Michalakos, P. M., Kung, M. C., Jahan, I., and Kung, H. H., *J. Catal.* **140,** 226 (1993).
44. Simakov, A. V., Sazonova, N. N., Ven'yaminov, S. A., Belomestnykh, I. P., Rozhdestvenskaya, N. N., and Isagulyants, G. V., *Kinet. Catal.* **30,** 598 (1989).
45. Akimoto, M., Usami, M., and Echigoya, E., *Bull. Chem. Soc. Jpn.* **51,** 2195 (1978).
46. Mori, K., Inomata, M., Miyamoto, A., and Murakami, Y., *J. Phys. Chem.* **87,** 4560 (1983).
47. Forzatti, P., Trifiró, F., and Villa, P. L., *J. Catal.* **52,** 389 (1978).
48. Busca, G., Lorenzelli, V., Oliveri, G., and Ramis, G., *in* "New Developments in Selective Oxidation II" (V. Cortés Corberán and S. Vic Bellón, Eds.), Studies in Surface Science and Catalysis, Vol. 82, p. 253. Elsevier, Amsterdam, 1994.